

# Dual Security for MIMO-OFDM ISAC Systems: Artificial Ghosts or Artificial Noise

Yinchao Yang, Prabhat Raj Gautam, Yathreb Bouazizi, Michael Breza, and Julie McCann

**Abstract**—Integrated sensing and communication (ISAC) enables the efficient sharing of wireless resources to support emerging applications, but it also gives rise to new sensing-based security vulnerabilities. Here, potential communication security threats whereby confidential messages intended for legitimate users are intercepted, but also unauthorized receivers (Eves) can passively exploit target echoes to infer sensing parameters without users being aware. Despite these risks, the joint protection of sensing and communication security in ISAC systems remains unexplored. To address this challenge, this paper proposes a two-layer dual-secure ISAC framework that simultaneously protects sensing and communication against passive sensing Eves and communication Eves, without requiring their channel state information (CSI). Specifically, transmit beamformers are jointly designed to inject artificial noise (AN) to introduce interference to communication Eves, while deliberately distorting the reference signal available to sensing Eves to impair their sensing capability. Furthermore, the proposed design generates artificial ghosts (AGs) with fake angle–range–velocity profiles observable by all receivers. Legitimate receivers can suppress these AGs, whereas sensing Eves cannot, thereby significantly reducing their probability of correctly detecting the true targets. Numerical results demonstrate that the proposed framework effectively enhances both communication and sensing security, while preserving the performance of communication users and legitimate sensing receivers.

**Index Terms**—ISAC, MIMO, OFDM, and physical layer security.

## I. INTRODUCTION

Integrated sensing and communication (ISAC) has been recognized by the International Telecommunication Union (ITU) as one of the key enabling technologies for sixth-generation (6G) wireless systems. By unifying sensing and communication within a common spectrum and hardware, ISAC enables the simultaneous transmission of information and perception of the surrounding environment [1]. More importantly, sensing and communication can mutually benefit from each other within the ISAC framework. On one hand, wireless sensing provides real-time environmental awareness, such as object locations and mobility states, which can be exploited by communication systems to perform adaptive beamforming, handover optimization, and interference management. On the other hand, communication enables sensing systems to exchange information for cooperative perception and network-level data fusion [2]. Millimeter-wave (mmWave)

ISAC enables a wide range of emerging applications, such as localization in autonomous vehicular networks [3] and vital-sign detection [4].

However, since the same signal is reused for both sensing and communication, ISAC systems are inherently exposed to physical-layer security vulnerabilities. The first security concern arises in the communication domain, where a communication eavesdropper (Eve) may intercept the transmitted waveform and attempt to recover confidential information when the encryption key is known or compromised. For instance, the target being detected by the transmitter can be the communication Eve who receives the joint signal and decodes confidential information, leading to data security concerns. The second and more distinctive threat lies in sensing security. Owing to the broadcast nature of electromagnetic (EM) waves, a sensing Eve can receive the reflected echoes from targets while simultaneously overhearing the direct-path signal from the transmitter as a reference waveform. By jointly processing the two signals, such as using a matched filter (MF), the sensing Eve can infer sensitive target information like velocity, geometric features, and even physiological information (e.g., respiration and heartbeat), thereby posing severe privacy risks.

Communication security in ISAC systems, also referred to as data or information security, has attracted significant research attention in recent years, resulting in a rich body of literature that establishes both solid theoretical foundations [5] and practical design methodologies [6]. In particular, a variety of physical-layer keyless security techniques have been developed to safeguard confidential information against passive eavesdropping. Representative approaches include information-theoretic secure designs [7], [8], artificial noise (AN) designs [9], [10], secure beamforming optimizations [11], [12], and waveform design methods [13], [14]. For active attacks, such as jamming and spoofing, in which an adversary deliberately injects interfering or deceptive signals to disrupt reliable reception or induce false information decoding, effective design methods have also been studied, e.g., [15], [16].

In contrast, sensing security, particularly sensing eavesdropping, is not yet mature in existing ISAC systems [17], [18]. Active sensing attacks, such as jamming and spoofing, can often be mitigated using defensive mechanisms developed for active communication attacks [19], [20]. In contrast, a passive sensing Eve does not transmit any signals, yet it can still infer sensitive physical-world information, thereby posing a fundamentally different and more challenging security threat. Existing defensive methods designed against passive communication Eves cannot be directly applied to sensing Eves. Moreover, unlike sensing-only systems, where secure

The authors are with the Department of Computing, Imperial College London, U.K., SW7 2AZ. (e-mail: yinchao.yang@imperial.ac.uk; p.gautam@imperial.ac.uk; y.bouazizi18@imperial.ac.uk; michael.breza04@imperial.ac.uk; j.mccann@imperial.ac.uk).

This work was supported by the EPSRC and DSIT through the Communications Hub for Empowering Distributed Cloud Computing Applications and Research (CHEDDAR) [grant numbers EP/X040518/1 and EP/Y037421/1].

designs based on radar-centric waveforms have been extensively investigated [21], [22], many ISAC frameworks employ communication-centric waveforms to simultaneously support sensing and data transmission. Such communication-centric signaling is inherently more vulnerable to sensing eavesdroppers due to the fundamental trade-off between sensing and communication under limited spectral and power resources. In contrast, radar-centric waveforms, such as FMCW, typically operate over wide bandwidths and exhibit low probability of interception (LPI) characteristics, while often requiring dedicated sensing hardware. Communication waveforms, however, are designed for interoperability across standard communication devices and are therefore more easily accessible to unauthorized receivers. Consequently, how to effectively prevent sensing eavesdropping in ISAC systems employing communication-centric waveforms remains largely unexplored [23], [24].

In this context, several recent studies have investigated sensing security against sensing Eves. In [25], illegal sensing is mitigated by minimizing the signal-to-noise ratio (SNR) at the sensing adversary while simultaneously minimizing the Cramér–Rao bound (CRB) at the legitimate sensing receiver to preserve sensing accuracy. In [26], a mutual-information (MI) based framework is developed, where the MI of the legitimate sensing receiver is maximized subject to constraints on the maximum allowable MI at the sensing Eves and the minimum signal-to-interference-plus-noise ratio (SINR) requirements of communication users to guarantee communication performance. Similarly, [27] maximizes the SNR of the legitimate sensing receiver to ensure sensing performance, while imposing SINR constraints for communication users and an upper bound on the sensing Eve’s SNR to achieve sensing security. A dual-secure design for cell-free ISAC networks is studied in [28]. However, the sensing Eve is assumed to have no access to the reference signal and can only perform non-coherent energy detection. Consequently, the detection probability of the sensing Eves is optimized, together with minimizing the SNR of the communication Eve to ensure communication security. Nevertheless, the above-mentioned works commonly rely on the assumption that the channel state information (CSI) of sensing Eves is perfectly known at the transmitter, which may be impractical in realistic deployments.

For the case where the CSI of sensing Eves is unknown, i.e., the sensing Eve-agnostic scenario, the authors in [29] enhance sensing security by minimizing the signal-to-artificial-noise ratio while maximizing the SNR of communication users to guarantee communication quality. However, data security against communication Eves and the sensing performance of the legitimate sensing receiver are not considered. In [30], artificial peaks are created via the ambiguity function (AF) to control the subcarrier power allocation in OFDM systems, resulting in the coexistence of actual and ghost targets in the sensing Eve’s range profile. Nevertheless, the ghost targets are confined to the range domain rather than the full angle–range–Doppler domain, making it easier for sensing Eves to correctly identify the true targets. Similarly, [31] investigates both OTFS and OFDM waveforms for sensing security by optimizing a Kullback–Leibler divergence–based detection met-

ric, such that strong sidelobes are induced in the sensing Eve’s range–Doppler profile to obscure the mainlobe. However, both works assume that the sensing Eve’s reference signal contains non-line-of-sight (NLoS) components that inherently degrade its quality. In practical scenarios, however, when the sensing Eve is located close to the transmitter, its reference signal may not experience strong NLoS distortion. In [32], sensing security in near-field ISAC systems is achieved by exploiting environmental scatter to mislead sensing eavesdroppers. This method relies on prior knowledge of the scatter information at the transmitter and assumes static scattering environments. Yet, these recent works focus solely on sensing security and do not explicitly consider communication security. An ISAC design considering dual security introduces further challenges and has not been addressed.

To bridge this research gap, where communication and sensing security must be jointly addressed in the absence of CSI of both communication and sensing Eves, we propose a dual-secure design against communication and sensing Eves, without the knowledge of their CSI, while guaranteeing the communication performance and sensing performance for communication users and legitimate sensing receivers, respectively. Our main contributions are summarized below:

- 1) We propose a secure MIMO-OFDM ISAC design that protects against both sensing and communication Eves without requiring their CSI. By injecting AN, communication Eves experience strong interference, thereby effectively reducing information leakage. Meanwhile, the injected AN also distorts the reference signal received by sensing Eves, which limits their estimation capabilities. This mechanism constitutes the first layer of sensing and communication security protection. However, in the case that if the sensing Eves are located close to the transmitter, their reference signal may remain of high quality. To address this case, a second layer of sensing security protection is introduced, which deliberately embeds artificial ghosts (AGs) with fake angle–delay–Doppler profiles into sensing Eves’ estimation results. This is achieved by designing the AF to generate artificial peaks in the angle–delay–Doppler domain, thereby misleading the sensing Eves toward ghost targets and reducing their probability of correctly detecting the true targets. With both defense mechanisms in place, sensing security is ensured regardless of the sensing Eve’s location or the quality of its received signals.
- 2) We establish performance measures for communication performance, communication security, sensing performance, and sensing security, respectively. With all the performance metrics, we formulate a four-way trade-off optimization problem that aims to maximize the sensing performance of the legitimate sensing receiver, subject to constraints on communication performance, communication security, and sensing security under limited resources. To tackle the resulting non-convex problem, several convex surrogate functions are introduced to obtain a tractable formulation. Simulation results verify the effectiveness of the proposed dual-secure design.

The remainder of this paper is organized as follows. Section II introduces the system model, including the underlying assumptions, the signal models of the transmitter and various receivers, and the associated signal processing procedures. Section III presents the performance metrics adopted in the design. Section IV formulates the proposed optimization problem and describes the solution. Section V provides numerical results to evaluate the performance of the proposed design. Finally, Section VI concludes the paper.

### List of Notations:

Capital boldface letters (e.g.,  $\mathbf{A}$ ) denote matrices, while lowercase boldface letters (e.g.,  $\mathbf{a}$ ) denote vectors. Scalars are represented using regular lowercase or uppercase fonts. The sets  $\mathbb{C}$ ,  $\mathbb{C}^{n \times 1}$ , and  $\mathbb{C}^{m \times n}$  represent a complex number, a complex vector of length  $n$ , and a complex  $m \times n$  matrix, respectively. The identity matrix is denoted by  $\mathbf{I}$ , and the zero matrix by  $\mathbf{0}$ . The notations  $[\cdot]^H$ ,  $\text{Tr}(\cdot)$ ,  $\text{rank}(\cdot)$ , and  $\text{blkdiag}(\cdot)$  represent the Hermitian transpose, the trace, the rank, and the block diagonal of a matrix, respectively. The  $l_2$  norm is denoted by  $\|\cdot\|$ . The symbol  $\succeq$  indicates positive semi-definite, while  $\odot$  and  $\otimes$  denote element-wise and Kronecker product, respectively. Finally,  $\mathcal{CN}(0, \sigma^2)$  represents a standard complex Gaussian distribution with zero mean and variance  $\sigma^2$ .

## II. SYSTEM MODEL

As illustrated in Fig. 1, we consider a monostatic mmWave ISAC base station (BS) equipped with  $N_t$  transmit antennas and  $N_r$  receive antennas, serving  $K$  communication users (CUs) each equipped with  $N_k$  antennas. The set of CU indices is denoted by  $\mathcal{K} \triangleq \{1, 2, \dots, K\}$ . In addition to communication, the BS performs radar sensing to localize  $L$  far-field, point-like targets, whose indices form the set  $\mathcal{L} \triangleq \{1, 2, \dots, L\}$ . In parallel, we consider the presence of sensing Eves equipped with  $N_{m_r}$  antennas that act as bistatic receivers attempting to intercept the target parameters from reflected echoes. The sensing Eve's index set is denoted by  $\mathcal{M}_r \triangleq \{1, 2, \dots, M_r\}$ . Likewise, a group of communication Eves attempts to overhear the downlink communication signals. Their index set is given by  $\mathcal{M}_c \triangleq \{1, 2, \dots, M_c\}$ , and each communication Eve is equipped with  $N_{m_c}$  antennas. Throughout this paper, we make the following assumptions:

**Assumption 1.** The sensing Eves can perfectly separate the reference signal from the surveillance signal via large antenna arrays (i.e.,  $N_{m_r} \gg N_t$ ), and they know the physical location of the BS.

**Assumption 2.** The BS has no knowledge of sensing or communication Eve's position or its existence.

**Assumption 3.** The BS knows the true angle of departure (AoD) of the targets, whereas sensing Eves do not.

**Assumption 4.** The sensing Eves can accurately estimate the angle-of-arrival (AoA) with respect to the targets.

Assumptions 1 and 2 correspond to a worst-case scenario in which sensing Eves remain completely passive while the BS

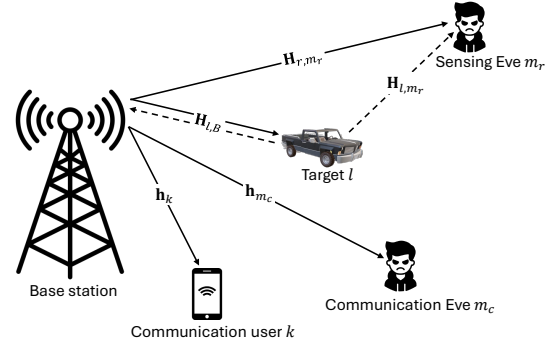


Fig. 1. A monostatic ISAC system with a target  $l \in \mathcal{L}$ , a communication user  $k \in \mathcal{K}$ , a bistatic sensing eavesdropper  $m_r \in \mathcal{M}_r$ , and a communication eavesdropper  $m_c \in \mathcal{M}_c$ .

continuously transmits signals, allowing any receiver to infer the BS location. Assumption 3 can be realized through an initial beam sweeping or omnidirectional transmission stage, enabling the BS to determine whether targets or objects exist within its coverage area. Assumption 4 also represents a worst-case scenario in which the sensing Eve can perfectly estimate the AoA, thereby posing a significant threat to the confidentiality of target location information.

### A. BS Transmit Signal Model

The ISAC BS employs an OFDM waveform to simultaneously serve CUs and illuminate the environment for sensing. Let  $\mathcal{N}_c$  and  $\mathcal{N}_s$  denote the sets of subcarrier and OFDM time slot indices, respectively. For each subcarrier-time slot pair  $(n_c, n_s)$ , the modulated symbol vector is  $\mathbf{s}_{n_c, n_s} = [s_{n_c, n_s, 1}, \dots, s_{n_c, n_s, K}]^T \in \mathbb{C}^{K \times 1}$ , where  $s_{n_c, n_s, k}$  denotes the modulated symbol of user  $k$ , drawn from a constellation set  $\mathcal{S}$ . The symbols are precoded and embedded with AN, resulting in the transmit signal:

$$\mathbf{x}_{n_c, n_s} = \mathbf{W}_{n_c, n_s} \mathbf{s}_{n_c, n_s} + \mathbf{q}_{n_c, n_s}, \quad (1)$$

where  $\mathbf{W}_{n_c, n_s} \in \mathbb{C}^{N_t \times K}$  is the beamforming matrix with each column  $\mathbf{w}_{n_c, n_s, k} \in \mathbb{C}^{N_t \times 1}$  being the beamforming vector of each user  $k$ , and  $\mathbf{q}_{n_c, n_s} \in \mathbb{C}^{N_t \times 1}$  is the AN vector. Following from [33], [34], we assume  $\mathbb{E}[\mathbf{s}_{n_c, n_s} \mathbf{s}_{n_c, n_s}^H] = \mathbf{I}$  and  $\mathbb{E}[\mathbf{s}_{n_c, n_s} \mathbf{q}_{n_c, n_s}^H] = \mathbf{0}$ , which indicates that the symbols are uncorrelated across users and are independent of the AN, respectively.

The corresponding baseband OFDM signal is given by [35]

$$\mathbf{x}(t) = \sum_{n_c \in \mathcal{N}_c} \sum_{n_s \in \mathcal{N}_s} \mathbf{x}_{n_c, n_s} e^{j2\pi n_c \Delta f t_{n_s}} \text{rect}\left(\frac{t_{n_s}}{T_{\text{tot}}}\right), \quad (2)$$

where  $t_{n_s} = t - n_s T_{\text{tot}}$ ,  $\Delta f = 1/T$  is the subcarrier spacing,  $T_{\text{tot}} = T + T_{\text{cp}}$  denotes the total symbol duration, with  $T$  and  $T_{\text{cp}}$  being the symbol duration and the cyclic prefix (CP) duration, respectively.

Finally, the baseband signal in (2) is up-converted to the carrier frequency  $f_c$ , resulting in the radio frequency (RF) domain transmit waveform  $\mathbf{x}_{\text{RF}}(t) = \mathbf{x}(t)e^{j2\pi f_c t}$ .

### B. BS Receive Signal Model

The BS observes echoes reflected by all targets in the set  $\mathcal{L}$ . The received RF domain signal can be expressed as

$$\begin{aligned} \mathbf{y}_{\text{RF},B}(t) &= \sum_{l \in \mathcal{L}} \mathbf{H}_{l,B} \mathbf{x}_{\text{RF}}(t - \tau_{l,B}) e^{j2\pi\mu_{l,B}t} + \mathbf{n}(t) \\ &= \sum_{l \in \mathcal{L}} \beta_{l,B} \mathbf{a}_r(\theta_{l,B}) \mathbf{a}_t^H(\theta_{l,t}) \mathbf{x}_{\text{RF}}(t - \tau_{l,B}) e^{j2\pi\mu_{l,B}t} + \mathbf{n}(t), \end{aligned} \quad (3)$$

where  $\beta_{l,B}$  denotes the complex path loss that incorporates propagation loss and the radar cross section (RCS) of the  $l$ -th target. The vectors  $\mathbf{a}_t(\theta_{l,t}) \in \mathbb{C}^{N_t \times 1}$  and  $\mathbf{a}_r(\theta_{l,B}) \in \mathbb{C}^{N_r \times 1}$  are the transmit and receive steering vectors evaluated at the angles from the BS to target  $l$  (i.e., AoD) and from target  $l$  to BS (i.e., AoA), respectively. The two-way trip delay is given by  $\tau_{l,B} = \frac{d_{t,l} + d_{l,B}}{c}$ , where  $d_{t,l}$  and  $d_{l,B}$  denote the propagation distances from the BS to the target and from the target to BS, respectively, and  $c$  is the speed of light. The Doppler shift associated with target  $l$  is  $\mu_{l,B} = \frac{(v_{t,l} + v_{l,B})f_c}{c}$ , with  $v_{t,l}$  and  $v_{l,B}$  representing the radial velocities along the BS–target and target–receiver directions, respectively. Finally,  $\mathbf{n}(t) \sim \mathcal{CN}(\mathbf{0}, \sigma_r^2 \mathbf{I}_{N_r})$  denotes the additive white Gaussian noise (AWGN).

After RF down-conversion, (3) becomes

$$\begin{aligned} \mathbf{y}_B(t) &= \sum_{l \in \mathcal{L}} \tilde{\beta}_{l,B} \mathbf{a}_r(\theta_{l,B}) \mathbf{a}_t^H(\theta_{l,t}) \sum_{n_c \in \mathcal{N}_c} \sum_{n_s \in \mathcal{N}_s} \mathbf{x}_{n_c, n_s} \\ &\cdot e^{j2\pi n_c \Delta f (t_{n_s} - \tau_{l,B})} e^{j2\pi \mu_{l,B} t} \text{rect}\left(\frac{t_{n_s} - \tau_{l,B}}{T_{\text{tot}}}\right) + \tilde{\mathbf{n}}(t), \end{aligned} \quad (4)$$

where  $\tilde{\beta}_{l,B} = \beta_{l,B} e^{-j2\pi f_c \tau_{l,B}}$  and  $\tilde{\mathbf{n}}(t) = \mathbf{n}(t) e^{-j2\pi f_c \tau_{l,B}}$ . We partition the received signal with respect to each symbol slot [36]:

$$\mathbf{y}_{n_s, B}(t) \triangleq \mathbf{y}_B(t + n_s T_{\text{tot}}), \forall n_s \in \mathcal{N}_s. \quad (5)$$

To obtain the discrete-time signal, we sample (5) with a sampling rate of  $f_s = N_c \Delta f$ . Accordingly, the  $p$ -th sample is given by

$$\begin{aligned} \mathbf{y}_{n_s, B}[p] &= \mathbf{y}_{n_s, B}(p/f_s) \\ &= \sum_{l \in \mathcal{L}} \tilde{\beta}_{l,B} \mathbf{a}_r(\theta_{l,B}) \mathbf{a}_t^H(\theta_{l,t}) \sum_{n_c \in \mathcal{N}_c} \mathbf{x}_{n_c, n_s} e^{j2\pi n_c \frac{p}{N_c}} \\ &\cdot e^{-j2\pi n_c \Delta f \tau_{l,B}} e^{j2\pi \mu_{l,B} \frac{p}{N_c \Delta f}} e^{j2\pi \mu_{l,B} n_s T_{\text{tot}}} + \tilde{\mathbf{n}}[p], \end{aligned} \quad (6)$$

with  $\tilde{\mathbf{n}}[p] = \tilde{\mathbf{n}}(\frac{p}{N_c \Delta f} + n_s T_{\text{tot}})$ . To avoid inter-carrier interference (ICI), the OFDM spacing must satisfy  $\mu_{l,B}/\Delta f \ll 1$ , as discussed in [37]. Thus, (6) can be approximated as

$$\begin{aligned} \mathbf{y}_{n_s, B}[p] &\approx \sum_{l \in \mathcal{L}} \tilde{\beta}_{l,B} \mathbf{a}_r(\theta_{l,B}) \mathbf{a}_t^H(\theta_{l,t}) \sum_{n_c \in \mathcal{N}_c} \mathbf{x}_{n_c, n_s} \\ &\cdot e^{j2\pi n_c \frac{p}{N_c}} e^{-j2\pi n_c \Delta f \tau_{l,B}} e^{j2\pi \mu_{l,B} n_s T_{\text{tot}}} + \tilde{\mathbf{n}}[p]. \end{aligned} \quad (7)$$

Then, by applying an  $N_c$ -point discrete Fourier transform (DFT) on (7), the received frequency-domain sample at sub-carrier  $n_c$  can be obtained as

$$\begin{aligned} \mathbf{y}_{n_c, n_s, B} &= \frac{1}{N_c} \sum_{p=0}^{N_c-1} \mathbf{y}_{n_s, B}[p] e^{-j2\pi n_c p / N_c} \\ &= \sum_{l \in \mathcal{L}} \tilde{\beta}_{l,B} \mathbf{a}_r(\theta_{l,B}) \mathbf{a}_t^H(\theta_{l,t}) \mathbf{x}_{n_c, n_s} e^{-j2\pi n_c \Delta f \tau_{l,B}} e^{j2\pi \mu_{l,B} n_s T_{\text{tot}}} + \bar{\mathbf{n}}, \end{aligned} \quad (8)$$

where  $\bar{\mathbf{n}}$  is the frequency-domain AWGN.

With (8), BS first estimates the AoA using high-resolution algorithms such as MUSIC [38]. Then, BS applies the spatial filtering applied to (8) yields the following result:

$$\begin{aligned} y_{n_c, n_s, B} &= \sum_{l \in \mathcal{L}} \tilde{\beta}_{l,B} \mathbf{a}_t^H(\theta_{l,t}) \mathbf{x}_{n_c, n_s} \\ &\cdot e^{-j2\pi n_c \Delta f \tau_{l,B}} e^{j2\pi \mu_{l,B} n_s T_{\text{tot}}} + \bar{n} \\ &= \sum_{l \in \mathcal{L}} \sum_{n_t \in \mathcal{N}_t} \frac{\tilde{\beta}_{l,B}}{\sqrt{N_t}} e^{-j2\pi \frac{d_t}{\lambda} \sin \theta_{l,t} n_t} \mathbf{x}_{n_c, n_s}[n_t] \\ &\cdot e^{-j2\pi n_c \Delta f \tau_{l,B}} e^{j2\pi \mu_{l,B} n_s T_{\text{tot}}} + \bar{n}, \end{aligned} \quad (9)$$

where  $\mathbf{x}_{n_c, n_s}[n_t]$  is the  $n_t$ -th element of the vector  $\mathbf{x}_{n_c, n_s}$ , and the antenna index is collected by the set  $\mathcal{N}_t$ .

**Remark 1.** In practical systems, all target parameters can be jointly estimated using multi-dimensional spectral estimation techniques, such as multi-dimensional periodograms or subspace-based methods. However, since the AoA is determined by the receiver side and is independent of transmitter side designs, we assume that the AoA has been accurately estimated beforehand. This allows the remaining parameter estimations to focus exclusively on delay, AoD, and Doppler, which are directly influenced by the transmit signal design.

### C. Sensing Eve Signal Model

The sensing Eve receives echo signals reflected from the targets through a bistatic propagation path. The received RF-domain signal is modeled as

$$\begin{aligned} \mathbf{y}_{\text{RF},m_r}(t) &= \sum_{l \in \mathcal{L}} \mathbf{H}_{l,m_r} \mathbf{x}_{\text{RF}}(t - \tau_{l,m_r}) e^{j2\pi \mu_{l,m_r} t} + \mathbf{n}(t) \\ &= \sum_{l \in \mathcal{L}} \beta_{l,m_r} \mathbf{a}_r(\theta_{l,m_r}) \mathbf{a}_t^H(\theta_{l,t}) \mathbf{x}_{\text{RF}}(t - \tau_{l,m_r}) e^{j2\pi \mu_{l,m_r} t} + \mathbf{n}(t), \end{aligned} \quad (10)$$

where  $\beta_{l,m_r}$  denotes the bistatic path loss,  $\theta_{l,m_r}$  represents the AoA from the  $l$ -th target to the  $m_r$ -th sensing Eve and  $\mathbf{a}_r(\theta_{l,m_r}) \in \mathbb{C}^{N_{m_r} \times 1}$  is the receive steering vector,  $\tau_{l,m_r}$  and  $\mu_{l,m_r}$  denote the corresponding time delay and Doppler shift, respectively, and  $\mathbf{n}(t)$  is AWGN.

1) *Reference Signal Reception:* Following **Assumption 1**, the sensing Eve is able to observe a reference signal directly from the BS. This observed signal is denoted by

$$\mathbf{y}_{r,m_r}(t) = \mathbf{H}_{r,m_r} \mathbf{x}_{\text{RF}}(t) + \mathbf{n}_{m_r}(t), \quad (11)$$

where  $\mathbf{H}_{r,m_r} \in \mathbb{C}^{N_{m_r} \times N_t}$  denotes the LoS channel between BS and the sensing Eve. Since the sensing Eve is aware of the transmitter's physical location, the reference signal can be obtained via the minimum variance unbiased (MVU) estimator [39], i.e.,  $\hat{\mathbf{x}}_{n_c, n_s} = (\mathbf{H}_{r,m_r}^H \mathbf{H}_{r,m_r})^{-1} \mathbf{H}_{r,m_r}^H \mathbf{y}_{r,m_r}(t)$ .

2) *Spatially Filtered Echo Signal:* By applying the same down-conversion, sampling, DFT, and spatial filtering steps as in BS's signal processing procedure, the sensing Eve obtains the following frequency-domain echo:

$$\begin{aligned} y_{n_c, n_s, m_r} &= \sum_{l \in \mathcal{L}} \sum_{n_t \in \mathcal{N}_t} \frac{\tilde{\beta}_{l,m_r}}{\sqrt{N_t}} e^{-j2\pi \frac{d_t}{\lambda} \sin \theta_{l,t} n_t} \mathbf{x}_{n_c, n_s}[n_t] \\ &\cdot e^{-j2\pi n_c \Delta f \tau_{l,m_r}} e^{j2\pi \mu_{l,m_r} n_s T_{\text{tot}}} + \bar{n}_{m_r}, \end{aligned} \quad (12)$$

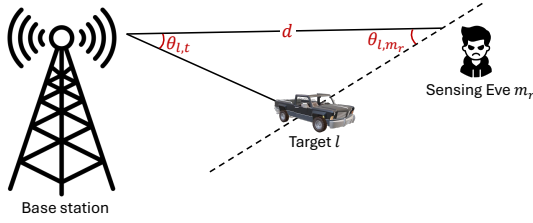


Fig. 2. Illustration of the sensing security vulnerability in an ISAC system. When only the distance  $d$  and the AoA angle  $\theta_{l,m_r}$  are exposed, the sensing Eve can infer that the target lies somewhere along the dotted locus but cannot determine its exact position. If the AoD  $\theta_{l,t}$  is also revealed, the target's location becomes fully identifiable.

where  $\tilde{\beta}_{l,m_r} = \beta_{l,m_r} e^{-j2\pi f_c \tau_{l,m_r}}$  and  $\bar{\mathbf{n}}_{m_r}$  denotes AWGN in the frequency domain.

**Remark 2.** Under the worst-case assumption where the transmitter's location is known to the sensing Eves (**Assumption 1**) and the adversary can accurately estimate the AoA (**Assumption 4**), the target must lie on a deterministic line (dotted line) as illustrated in Fig. 2. Consequently, it is essential to prevent the adversary from recovering  $\theta_{l,t}$ ,  $\tau_{l,m_r}$ , and  $\mu_{l,m_r}$ , since these parameters provide additional geometric information that enables localization of the target. For example, knowing two angles and one side of a triangle allows the target position to be uniquely determined.

#### D. Echo Signal Processing

For the BS and the sensing Eves, the objective is to detect the presence of targets and, upon detection, to estimate their physical parameters. The parameters of interest are defined as  $\Psi_B = [\theta_{l,t}, \tau_{l,B}, \mu_{l,B}]$  and  $\Psi_{m_r} = [\theta_{l,t}, \tau_{l,m_r}, \mu_{l,m_r}]$ ,  $\forall l \in \mathcal{L}$ , respectively.

For design traceability, we assume that the delay and Doppler shifts lie on the discrete resolution grid [40]. That is,  $\tau_l = \frac{\ell_l}{N_c \Delta f}$ ,  $\mu_l = \frac{\nu_l}{N_s T_{\text{tot}}}$ , where  $\ell_l$  and  $\nu_l$  denote the delay and Doppler bins, respectively. Therefore, the signals in (9) and (12) can be written in matrix form as

$$\mathbf{Y}_i = \sum_{l \in \mathcal{L}} \tilde{\beta}_{l,i} \mathbf{D}_{\ell_{l,i}} \tilde{\mathbf{X}}_l \mathbf{D}_{\nu_{l,i}} + \mathbf{N}, \quad i \in [B, m_r], \quad (13)$$

where

$$\begin{cases} \mathbf{Y}_i[n_c, n_s] = y_{n_c, n_s, i}, \\ \tilde{\mathbf{X}}_l = (\mathbf{I}_{N_c} \otimes \mathbf{a}_t^H(\theta_{l,t})) \mathbf{X}, \quad \mathbf{X} \in \mathbb{C}^{N_c N_t \times N_s}, \\ \mathbf{D}_{\ell_{l,i}} = \text{diag} \left( 1, e^{-j2\pi \ell_{l,i} \frac{1}{N_c}}, \dots, e^{-j2\pi \ell_{l,i} \frac{N_c-1}{N_c}} \right), \\ \mathbf{D}_{\nu_{l,i}} = \text{diag} \left( 1, e^{j2\pi \nu_{l,i} \frac{1}{N_s}}, \dots, e^{j2\pi \nu_{l,i} \frac{N_s-1}{N_s}} \right). \end{cases}$$

To estimate  $\Psi_i$ , we employ a three-dimensional MF across angle, delay, and Doppler domains. The MF output is given by [41]

$$\hat{\Psi}_i = (\mathbf{F}_{N_c}^H (\mathbf{Y}_i \odot (\mathbf{F}_\theta \mathbf{X}_i^*)) \mathbf{F}_{N_s}), \quad i \in [B, m_r], \quad (14)$$

where  $\mathbf{F}_{N_c}$  and  $\mathbf{F}_{N_s}$  denote the DFT matrices for delay and Doppler processing,  $\mathbf{F}_\theta$  is the steering matrix, and  $\hat{\Psi}_i = [\hat{\theta}_{l,t}, \hat{\tau}_{l,i}, \hat{\mu}_{l,i}]$  contains the estimated parameters.

#### E. Communication Models

For a communication user  $k \in \mathcal{K}$ , the received time-domain signal is given by

$$\mathbf{y}_k(t) = \mathbf{H}_k \mathbf{x}(t) + \mathbf{n}_k(t), \quad (15)$$

where  $\mathbf{H}_k \in \mathbb{C}^{N_k \times N_t}$  is the channel between transmitter and user  $k$ , and  $\mathbf{n}_k \sim \mathcal{CN}(0, \sigma_c^2 \mathbf{I})$  is AWGN. Following the similar OFDM signal processing procedure as shown in (4)-(8), the received frequency domain signal is given by

$$\mathbf{y}_{n_c, n_s, k} = \mathbf{H}_{n_c, n_s, k} \mathbf{x}_{n_c, n_s} + \bar{\mathbf{n}}_k, \quad (16)$$

where  $\mathbf{H}_{n_c, n_s, k} \in \mathbb{C}^{N_k \times N_t}$  denotes the downlink channel vector on subcarrier  $n_c$  and symbol  $n_s$ , and  $\bar{\mathbf{n}}_k$  is AWGN. Perfect CSI is assumed at the BS, obtainable through standard uplink-downlink pilot estimation prior to the beamforming design.

Substituting (1) into (16), we can decompose the received signal as

$$\begin{aligned} \mathbf{y}_{n_c, n_s, k} = & \underbrace{\mathbf{H}_{n_c, n_s, k} \mathbf{w}_{n_c, n_s, k} s_{n_c, n_s, k}}_{\text{Desired signal}} \\ & + \underbrace{\sum_{k' \in \mathcal{K}, k' \neq k} \mathbf{H}_{n_c, n_s, k} \mathbf{w}_{n_c, n_s, k'} s_{n_c, n_s, k'}}_{\text{Multi-user interference}} \\ & + \underbrace{\mathbf{H}_{n_c, n_s, k} \mathbf{q}_{n_c, n_s}}_{\text{Artificial noise}} + \bar{\mathbf{n}}_k, \end{aligned} \quad (17)$$

where  $\mathbf{w}_{n_c, n_s, k} \in \mathbb{C}^{N_t \times 1}$  is the  $k$ -th column of  $\mathbf{W}_{n_c, n_s}$ .

For the communication Eve  $m_c \in \mathcal{M}_c$ , its intercepted signal in the time-domain is given by

$$\mathbf{y}_{m_c}(t) = \mathbf{H}_{m_c} \mathbf{x}(t) + \mathbf{n}_{m_c}(t), \quad (18)$$

where  $\mathbf{H}_{m_c} \in \mathbb{C}^{N_{m_c} \times N_t}$  is the channel between transmitter and communication Eve  $m_c$ , and  $\mathbf{n}_{m_c} \sim \mathcal{CN}(0, \sigma_c^2 \mathbf{I})$  is AWGN. After standard OFDM procedures, the intercepted signal in relation to the  $k$ -th CU is given by

$$\begin{aligned} \mathbf{y}_{n_c, n_s, k, m_c} = & \underbrace{\mathbf{H}_{n_c, n_s, m_c} \mathbf{w}_{n_c, n_s, k} s_{n_c, n_s, k}}_{\text{Intercepted signal}} \\ & + \underbrace{\sum_{k' \in \mathcal{K}, k' \neq k} \mathbf{H}_{n_c, n_s, m_c} \mathbf{w}_{n_c, n_s, k'} s_{n_c, n_s, k'}}_{\text{Multi-user interference}} \\ & + \underbrace{\mathbf{H}_{n_c, n_s, m_c} \mathbf{q}_{n_c, n_s}}_{\text{Artificial noise}} + \bar{\mathbf{n}}_{m_c}, \end{aligned} \quad (19)$$

where  $\mathbf{H}_{n_c, n_s, m_c} \in \mathbb{C}^{N_{m_c} \times N_t}$  denotes the downlink channel vector on subcarrier  $n_c$  and symbol  $n_s$  for the communication Eve  $m_c \in \mathcal{M}_c$ .

### III. PERFORMANCE METRICS

In this section, we present the performance metrics for sensing, communication, and security, respectively.

TABLE I  
DESIRED AMBIGUITY FUNCTION BEHAVIOR FOR BS AND THE SENSING EVE

	Mainlobe(s)	Sidelobe(s)
BS	$ \chi(0, 0, \theta_{l,t}, \theta_{l,t}) ^2 = 1$	$ \chi(\Delta\ell \neq 0, \Delta\nu \neq 0, \theta_{l,t}, \hat{\theta}_{l,t} \neq \theta_{l,t}) ^2 = 0$
The sensing Eve	$ \chi(\Delta\ell \neq 0, \Delta\nu \neq 0, \theta_{l,t}, \hat{\theta}_{l,t} \neq \theta_{l,t}) ^2 = 1$	$ \chi(0, 0, \theta_{l,t}, \theta_{l,t}) ^2 = 0$

### A. Sensing Accuracy for BS

To characterize the sensing capability of the BS, we consider the post-MF SNR evaluated at the correct delay, Doppler, and angle, i.e.,  $\hat{\tau}_{l,B} = \tau_{l,B}$ ,  $\hat{\nu}_{l,B} = \nu_{l,B}$  and  $\hat{\theta}_{l,t} = \theta_{l,t}$ . Since BS possesses perfect knowledge of the reference signal without AN, the resulting post-MF SNR at each  $(n_c, n_s)$  resource block of target  $l$  can be expressed as

$$\gamma_{n_c, n_s, l, B} = \frac{\tilde{\beta}_{l,B}^2 \|\mathbf{a}_r^H(\theta_{l,B})\|^2 \|\mathbf{a}_t^H(\theta_{l,t}) \mathbf{W}_{n_c, n_s}\|^2}{\sigma_r^2}. \quad (20)$$

### B. Sensing Security using Artificial Ghosts

The MF operation expressed in (14) is employed to efficiently estimate the target parameters. For analytical purposes and assuming the worst-case where sensing Eve's estimated reference signal is error-free, i.e.,  $\hat{\mathbf{x}}_{n_c, n_s} = \mathbf{x}_{n_c, n_s}$ , we rewrite the MF output explicitly as

$$\begin{aligned} \chi(\hat{\ell}_l, \hat{\nu}_l, \theta_{l,t}, \hat{\theta}_{l,t}) &= \sum_{n'_t \in \mathcal{N}_t} \sum_{n_c \in \mathcal{N}_c} \sum_{n_s \in \mathcal{N}_s} y_{n_c, n_s} \mathbf{x}_{n_c, n_s}^* [n'_t] \\ &\cdot \frac{1}{\sqrt{N_t}} e^{j2\pi \frac{d_t}{\lambda} \sin \hat{\theta}_{l,t} n'_t} e^{j2\pi \hat{\ell}_l \frac{n_c}{N_c}} e^{-j2\pi \hat{\nu}_l \frac{n_s}{N_s}}. \end{aligned} \quad (21)$$

By substituting (12) into (21), it can be observed that the MF output depends explicitly on  $\mathbf{W}_{n_c, n_s}$  and  $\mathbf{q}_{n_c, n_s}$ . This naturally leads to the characterization of the ambiguity function (AF), which describes the autocorrelation of the transmitted and received ISAC signal across angle, delay, and Doppler [30], [42]. By neglecting the path loss coefficients and noise terms, and substituting into (21), we obtain the expected AF expression shown in (22). The notations used in (22) are given below:

$$\begin{cases} \mathbf{A}(\Delta\ell, \Delta\nu, \theta_{l,t}, \hat{\theta}_{l,t}) = \frac{1}{N_t} \mathbf{a}_t(\theta_{l,t}) \mathbf{a}_t^H(\hat{\theta}_{l,t}) e^{-j2\pi \frac{n_c}{N_c} (\Delta\ell)} e^{j2\pi \frac{n_s}{N_s} (\Delta\nu)}, \\ \bar{\mathbf{A}}(\theta_{l,t}) = \frac{1}{\sqrt{N_t}} \mathbf{a}_t(\theta_{l,t}) \otimes \mathbf{I}_{N_c N_s}, \\ \bar{\mathbf{W}}_{n_c, n_s} \in \mathbb{C}^{N_t \times N_t} = \mathbf{W}_{n_c, n_s} \mathbf{W}_{n_c, n_s}^H, \\ \bar{\mathbf{W}} = \text{blkdiag}(\bar{\mathbf{W}}_{1,1}, \dots, \bar{\mathbf{W}}_{N_c, N_s}), \\ \mathbf{Q}_{n_c, n_s} \in \mathbb{C}^{N_t \times N_t} = \mathbf{q}_{n_c, n_s} \mathbf{q}_{n_c, n_s}^H, \\ \bar{\mathbf{Q}} = \text{blkdiag}(\mathbf{Q}_{1,1}, \dots, \mathbf{Q}_{N_c, N_s}), \end{cases}$$

and  $\mathbf{D}_{\Delta\ell}$ ,  $\mathbf{D}_{\Delta\nu}$  has been defined in (13).

As summarized in Table I, and assuming that (22) is normalized to lie within  $[0, 1]$  after squaring, achieving high sensing accuracy for BS and ensuring sensing security against Eve constitute two inherently contrasting design objectives. Since (22) is determined by  $\bar{\mathbf{W}}$  and  $\mathbf{Q}$  that are observed by all receivers, these objectives are fundamentally conflicting.

To navigate this tradeoff, we aim to design the beamformers such that BS retains a dominant and unambiguous mainlobe at the true target location, while the sensing Eves are diverted toward AGs, thereby reducing their probability of correctly detecting the actual target.

As such, we consider the PSL [43] and the ISL [37] that quantify the highest sidelobe peak and the total sidelobe energy relative to the mainlobe, respectively. The PSL formulation is given by

$$\text{PSL}_l = \frac{|\chi(\Delta\ell_g, \Delta\nu_g, \theta_{l,t}, \theta_{g,t})|^2}{|\chi(0, 0, \theta_{l,t}, \theta_{l,t})|^2} \geq \eta_{\text{PSL}}, \forall g \in \mathcal{G}, g \notin \mathcal{L} \cup \mathcal{K}, \quad (23)$$

where  $\mathcal{G}$  denotes the set of AG indices, and each ghost has the delay-Doppler-angle coordinates of  $(\Delta\ell_g, \Delta\nu_g, \theta_{g,t})$ . And the ISL formulation is given by:

$$\text{ISL}_l = \frac{\sum_{\hat{\theta}_{l,t}} \sum_{\substack{\Delta\ell=0, \Delta\nu=0 \\ (\Delta\ell, \Delta\nu) \neq (0,0)}}^{N_c-1, N_s-1} |\chi(\Delta\ell, \Delta\nu, \theta_{l,t}, \hat{\theta}_{l,t})|^2}{|\chi(0, 0, \theta_{l,t}, \theta_{l,t})|^2} \geq \eta_{\text{ISL}}, \quad (24)$$

where  $\hat{\theta}_{l,t} \in [-\frac{\pi}{2}, \frac{\pi}{2}]$ ,  $\hat{\theta}_{l,t} \neq \theta_{l,t}$ .

### C. Sensing Security Using Artificial Noise

AN is used to deliberately distort the reference signal observed by a potential sensing Eve, as shown in (11). To quantify the resulting degradation in Eve's sensing capability under the MIMO setting (**Assumption 1**), we consider the average data rate at a hypothetical Eve located at angle  $\theta_{m_r}$ :

$$\begin{aligned} C_{m_r} &= \frac{1}{N_c N_s} \sum_{\substack{n_c \in \mathcal{N}_c, \\ n_s \in \mathcal{N}_s}} \log \det \left( \mathbf{I} + \frac{\mathbf{H}_{r, m_r} \bar{\mathbf{W}}_{n_c, n_s} \mathbf{H}_{r, m_r}^H}{\mathbf{H}_{r, m_r} \mathbf{Q}_{n_c, n_s} \mathbf{H}_{r, m_r}^H + \sigma_e^2 \mathbf{I}} \right), \end{aligned} \quad (25)$$

where  $\mathbf{H}_{r, m_r} = \mathbf{a}_r(\theta_{m_r}) \mathbf{a}_t^H(\theta_{m_r})$ , with  $\theta_{m_r} \in [-\frac{\pi}{2}, \frac{\pi}{2}]$ ,  $\theta_{m_r} \notin \mathcal{K}$  denoting the angular location of a potential sensing Eve. We note that the path loss effect is omitted in (25) due to the lack of knowledge about Eve's distance (i.e., **Assumption 2**). As a result, (25) characterizes the best-case sensing capability of Eve. In practice, propagation loss would further attenuate the received signal and hence reduce the performance for sensing Eves [29], [44].

### D. Communication Performance and Security

Based on the signal model in (17), the average data rate of the  $k$ -th CU is expressed in (26), where  $\mathbf{W}_{n_c, n_s, k} = \mathbf{w}_{n_c, n_s, k} \mathbf{w}_{n_c, n_s, k}^H$  and  $\mathbf{Q}_{n_c, n_s} = \mathbf{q}_{n_c, n_s} \mathbf{q}_{n_c, n_s}^H$ .

$$\begin{aligned}
 \chi(\hat{\ell}_l, \hat{\nu}_l, \theta_{l,t}, \hat{\theta}_{l,t}) &= \frac{1}{N_t} \mathbb{E} \left\{ \sum_{n_t, n'_t \in \mathcal{N}_t} \sum_{n_c \in \mathcal{N}_c} \sum_{n_s \in \mathcal{N}_s} e^{-j2\pi \frac{d_t}{\lambda} \sin \theta_{l,t} n_t} \mathbf{x}_{n_c, n_s}[n_t] e^{-j2\pi \ell_l \frac{n_c}{N_c}} e^{j2\pi \nu_l \frac{n_s}{N_s}} \right. \\
 &\quad \left. \cdot \mathbf{x}_{n_c, n_s}^*[n'_t] e^{j2\pi \frac{d_t}{\lambda} \sin \hat{\theta}_{l,t} n'_t} e^{j2\pi \hat{\ell}_l \frac{n_c}{N_c}} e^{-j2\pi \hat{\nu}_l \frac{n_s}{N_s}} \right\} \\
 &= \frac{1}{N_t} \mathbb{E} \left\{ \sum_{n_c \in \mathcal{N}_c} \sum_{n_s \in \mathcal{N}_s} \mathbf{x}_{n_c, n_s}^H \mathbf{a}_t(\theta_{l,t}) \mathbf{a}_t^H(\hat{\theta}_{l,t}) \mathbf{x}_{n_c, n_s} e^{-j2\pi \frac{n_c}{N_c} (\Delta \ell)} e^{j2\pi \frac{n_s}{N_s} (\Delta \nu)} \right\} \\
 &= \sum_{n_c \in \mathcal{N}_c} \sum_{n_s \in \mathcal{N}_s} \text{Tr} \left( \mathbf{A}(\Delta \ell, \Delta \nu, \theta_{l,t}, \hat{\theta}_{l,t}) \bar{\mathbf{W}}_{n_c, n_s} \right) + \text{Tr} \left( \mathbf{A}(\Delta \ell, \Delta \nu, \theta_{l,t}, \hat{\theta}_{l,t}) \mathbf{Q}_{n_c, n_s} \right) \\
 &= \text{Tr} \left( \bar{\mathbf{A}}(\theta_{l,t}) (\mathbf{D}_{\Delta \ell} \otimes \mathbf{D}_{\Delta \nu}) \bar{\mathbf{A}}^H(\hat{\theta}_{l,t}) \bar{\mathbf{W}} \right) + \text{Tr} \left( \bar{\mathbf{A}}(\theta_{l,t}) (\mathbf{D}_{\Delta \ell} \otimes \mathbf{D}_{\Delta \nu}) \bar{\mathbf{A}}^H(\hat{\theta}_{l,t}) \bar{\mathbf{Q}} \right) \triangleq \chi(\Delta \ell, \Delta \nu, \theta_{l,t}, \hat{\theta}_{l,t}). \quad (22)
 \end{aligned}$$

$$C_k = \frac{1}{N_c N_s} \sum_{\substack{n_c \in \mathcal{N}_c, \\ n_s \in \mathcal{N}_s}} \log \det \left( \mathbf{I} + \mathbf{H}_{n_c, n_s, k} \mathbf{W}_{n_c, n_s, k} \mathbf{H}_{n_c, n_s, k}^H \left( \mathbf{H}_{n_c, n_s, k} \left( \sum_{\substack{k' \in \mathcal{K}, \\ k' \neq k}} \mathbf{W}_{n_c, n_s, k'} + \mathbf{Q}_{n_c, n_s} \right) \mathbf{H}_{n_c, n_s, k}^H + \sigma_c^2 \mathbf{I} \right)^{-1} \right), \quad (26)$$

$$C_{k, m_c} = \frac{1}{N_c N_s} \sum_{\substack{n_c \in \mathcal{N}_c, \\ n_s \in \mathcal{N}_s}} \log \det \left( \mathbf{I} + \mathbf{H}_{n_c, n_s, m_c} \mathbf{W}_{n_c, n_s, k} \mathbf{H}_{n_c, n_s, m_c}^H \left( \mathbf{H}_{n_c, n_s, m_c} \left( \sum_{\substack{k' \in \mathcal{K}, \\ k' \neq k}} \mathbf{W}_{n_c, n_s, k'} + \mathbf{Q}_{n_c, n_s} \right) \mathbf{H}_{n_c, n_s, m_c}^H + \sigma_c^2 \mathbf{I} \right)^{-1} \right), \quad (27)$$

For a communication Eve indexed by  $m_c \in \mathcal{M}_c$ , its data rate is shown in (27), where  $\mathbf{H}_{n_c, n_s, m_c} = \mathbf{a}_r^H(\theta_{m_c}) \mathbf{a}_t(\theta_{m_c})$ , with  $\theta_{m_c} \in [-\frac{\pi}{2}, \frac{\pi}{2}]$ ,  $\theta_{m_c} \notin \mathcal{K}$  denoting the angular location of a potential communication Eve.

Finally, the worst-case secrecy rate of the  $k$ -th CU, which quantifies the communication security, is given by

$$S_k = \min_{m_c \in \mathcal{M}_c} [C_k - C_{k, m_c}]^+, \quad (28)$$

where  $[A]^+$  means  $\max(A, 0)$ .

#### IV. DUAL SECURE DESIGN FOR MIMO-OFDM ISAC SYSTEMS

This section formulates the dual-secure ISAC design problem and proposes an algorithm for solving the resulting nonconvex problem.

##### A. Problem Formulation

The design objective is to ensure reliable sensing performance while simultaneously guaranteeing communication performance, sensing security, and communication security. Accordingly, the optimization problem is formulated based on

the aforementioned performance metrics and is presented as follows:

$$\max_{\mathbf{W}_{n_c, n_s, k}, \mathbf{Q}_{n_c, n_s}, \eta_B} \eta_B \quad (29a)$$

$$\text{s.t. } \gamma_{n_c, n_s, l, B} \geq \eta_B, \forall n_c \in \mathcal{N}_c, \forall n_s \in \mathcal{N}_s, \forall l \in \mathcal{L}, \quad (29b)$$

$$C_{m_r} \leq \eta_E, \forall m_r \in \mathcal{M}_r, \quad (29c)$$

$$\text{PSL}_l \geq \eta_{\text{PSL}}, \forall l \in \mathcal{L}, \quad (29d)$$

$$\text{ISL}_l \geq \eta_{\text{ISL}}, \forall l \in \mathcal{L}, \quad (29e)$$

$$S_k \geq \eta_s, \forall k \in \mathcal{K}, \quad (29f)$$

$$\sum_{n_c \in \mathcal{N}_c} \sum_{n_s \in \mathcal{N}_s} \text{Tr} \left( \sum_{k \in \mathcal{K}} \mathbf{W}_{n_c, n_s, k} + \mathbf{Q}_{n_c, n_s} \right) \leq P_t, \quad (29g)$$

$$\mathbf{W}_{n_c, n_s, k} \succeq 0, \mathbf{Q}_{n_c, n_s} \succeq 0, \quad (29h)$$

$$\text{rank}(\mathbf{W}_{n_c, n_s, k}) = 1. \quad (29i)$$

The objective function in (29a), together with constraint (29b), is designed to maximize the BS's sensing performance as quantified in (20). Constraint (29c) limits the quality of the sensing Eve's reference signal, thereby deliberately impairing its sensing capability. Constraint (29d) facilitates the generation of AGs, whereas constraint (29e) controls sidelobe levels to promote energy focusing on the true targets and AGs. Constraint (29f) ensures secure communication, and constraint (29g) enforces the transmit power budget  $P_t$ . Lastly, constraints (29h) and (29i) guarantee that the resulting matrices are decomposable into feasible per-user beamforming structures. Following from [45], [46], we drop the rank-one constraint due to its non-convex behavior. A rank-one solution

$$\begin{aligned}
 & \frac{1}{N_c N_s} \sum_{n_c \in \mathcal{N}_c, n_s \in \mathcal{N}_s} \log \det \left( \mathbf{H}_{r,m_r} \left( \bar{\mathbf{W}}_{n_c, n_s}^{(e)} + \mathbf{Q}_{n_c, n_s}^{(e)} \right) \mathbf{H}_{r,m_r}^H + \sigma_c^2 \mathbf{I} \right) \\
 & + \text{Tr} \left( \left( \mathbf{H}_{r,m_r} \left( \bar{\mathbf{W}}_{n_c, n_s}^{(e)} + \mathbf{Q}_{n_c, n_s}^{(e)} \right) \mathbf{H}_{r,m_r}^H + \sigma_c^2 \mathbf{I} \right)^{-1} \left( \mathbf{H}_{r,m_r} \left( \bar{\mathbf{W}}_{n_c, n_s} - \bar{\mathbf{W}}_{n_c, n_s}^{(e)} + \mathbf{Q}_{n_c, n_s} - \mathbf{Q}_{n_c, n_s}^{(e)} \right) \mathbf{H}_{r,m_r}^H \right) \right) \\
 & - \log \det \left( \mathbf{H}_{r,m_r} \mathbf{Q}_{n_c, n_s} \mathbf{H}_{r,m_r}^H + \sigma_c^2 \mathbf{I} \right) \leq \eta_E, \tag{30}
 \end{aligned}$$

$$\begin{aligned}
 & \eta_{\text{PSL}} \left| \text{Tr} \left( \bar{\mathbf{A}}(\theta_{l,t}) \bar{\mathbf{A}}^H(\theta_{l,t}) \bar{\mathbf{W}} \right) + \text{Tr} \left( \bar{\mathbf{A}}(\theta_{l,t}) \bar{\mathbf{A}}^H(\theta_{l,t}) \bar{\mathbf{Q}} \right) \right|^2 - \left( \left| f_{\text{PSL}}(\bar{\mathbf{W}}^{(e)}, \bar{\mathbf{Q}}^{(e)}) \right|^2 + 2\Re \left\{ f_{\text{PSL}}^*(\bar{\mathbf{W}}^{(e)}, \bar{\mathbf{Q}}^{(e)}) \right. \right. \\
 & \cdot \left. \left. \left[ \text{Tr} \left( \bar{\mathbf{A}}(\theta_{l,t}) (\mathbf{D}_{\ell_g} \otimes \mathbf{D}_{\nu_g}) \bar{\mathbf{A}}^H(\theta_{g,t}) (\bar{\mathbf{W}} - \bar{\mathbf{W}}^{(e)}) \right) + \text{Tr} \left( \bar{\mathbf{A}}(\theta_{l,t}) (\mathbf{D}_{\ell_g} \otimes \mathbf{D}_{\nu_g}) \bar{\mathbf{A}}^H(\theta_{g,t}) (\bar{\mathbf{Q}} - \bar{\mathbf{Q}}^{(e)}) \right) \right] \right\} \right) \leq 0, \tag{31} \\
 & \text{where } f_{\text{PSL}}(\bar{\mathbf{W}}^{(e)}, \bar{\mathbf{Q}}^{(e)}) \triangleq \text{Tr} \left( \bar{\mathbf{A}}(\theta_{l,t}) (\mathbf{D}_{\ell_g} \otimes \mathbf{D}_{\nu_g}) \bar{\mathbf{A}}^H(\theta_{g,t}) \bar{\mathbf{W}}^{(e)} \right) + \text{Tr} \left( \bar{\mathbf{A}}(\theta_{l,t}) (\mathbf{D}_{\ell_g} \otimes \mathbf{D}_{\nu_g}) \bar{\mathbf{A}}^H(\theta_{g,t}) \bar{\mathbf{Q}}^{(e)} \right).
 \end{aligned}$$

$$\begin{aligned}
 & \eta_{\text{ISL}} \left| \text{Tr} \left( \bar{\mathbf{A}}(\theta_{l,t}) \bar{\mathbf{A}}^H(\theta_{l,t}) \bar{\mathbf{W}} \right) + \text{Tr} \left( \bar{\mathbf{A}}(\theta_{l,t}) \bar{\mathbf{A}}^H(\theta_{l,t}) \bar{\mathbf{Q}} \right) \right|^2 - \sum_{\hat{\theta}_{l,t}} \sum_{\Delta \ell=1}^{N_c-1} \sum_{\Delta \nu=1}^{N_s-1} \left( \left| f_{\text{ISL}}(\bar{\mathbf{W}}^{(e)}, \bar{\mathbf{Q}}^{(e)}) \right|^2 + 2\Re \left\{ f_{\text{ISL}}^*(\bar{\mathbf{W}}^{(e)}, \bar{\mathbf{Q}}^{(e)}) \right. \right. \\
 & \cdot \left. \left. \left[ \text{Tr} \left( \bar{\mathbf{A}}(\theta_{l,t}) (\mathbf{D}_{\Delta \ell} \otimes \mathbf{D}_{\Delta \nu}) \bar{\mathbf{A}}^H(\hat{\theta}_{l,t}) (\bar{\mathbf{W}} - \bar{\mathbf{W}}^{(e)}) \right) + \text{Tr} \left( \bar{\mathbf{A}}(\theta_{l,t}) (\mathbf{D}_{\Delta \ell} \otimes \mathbf{D}_{\Delta \nu}) \bar{\mathbf{A}}^H(\hat{\theta}_{l,t}) (\bar{\mathbf{Q}} - \bar{\mathbf{Q}}^{(e)}) \right) \right] \right\} \right) \leq 0, \tag{32} \\
 & \text{where } f_{\text{ISL}}(\bar{\mathbf{W}}^{(e)}, \bar{\mathbf{Q}}^{(e)}) \triangleq \text{Tr} \left( \bar{\mathbf{A}}(\theta_{l,t}) (\mathbf{D}_{\Delta \ell} \otimes \mathbf{D}_{\Delta \nu}) \bar{\mathbf{A}}^H(\hat{\theta}_{l,t}) \bar{\mathbf{W}}^{(e)} \right) + \text{Tr} \left( \bar{\mathbf{A}}(\theta_{l,t}) (\mathbf{D}_{\Delta \ell} \otimes \mathbf{D}_{\Delta \nu}) \bar{\mathbf{A}}^H(\hat{\theta}_{l,t}) \bar{\mathbf{Q}}^{(e)} \right).
 \end{aligned}$$

can be recovered from the optimal solutions via Gaussian randomization.

### B. Problem Transformation

The optimization problem is non-convex due to the constraints in (29c)–(29f). We first consider constraint (29c). By rewriting (29c) in a difference-of-convex (DC) form [47] and applying a first-order Taylor approximation to its concave component, a convex surrogate constraint is obtained, as shown in (30). The matrices  $\bar{\mathbf{W}}_{n_c, n_s}^{(e)}$  and  $\mathbf{Q}_{n_c, n_s}^{(e)}$  are updated iteratively.

Using the same approach, constraint (29d) is reformulated into a DC representation and subsequently approximated via a first-order Taylor expansion, leading to the convex surrogate in (31). In this step, the auxiliary matrices  $\bar{\mathbf{W}}^{(e)}$  and  $\bar{\mathbf{Q}}^{(e)}$  are constructed from  $\bar{\mathbf{W}}_{n_c, n_s}^{(e)}$  and  $\mathbf{Q}_{n_c, n_s}^{(e)}$ .

Constraint (29e) already admits a DC structure and can therefore be directly approximated by a convex surrogate, as given in (32).

Finally, following the same procedure as for (29c), constraint (29f) is approximated by the convex surrogate shown in (33).

Therefore, problem (29) has been equivalently reformulated as the following convex optimization problem:

$$\max_{\mathbf{W}_{n_c, n_s, k}, \mathbf{Q}_{n_c, n_s}, \eta_B} \eta_B \tag{34a}$$

$$\text{s.t. } \gamma_{n_c, n_s, l, B} \geq \eta_B, \forall n_c \in \mathcal{N}_c, \forall n_s \in \mathcal{N}_s, \forall l \in \mathcal{L}, \tag{34b}$$

$$(30), (31), (32), (33), (29g). \tag{34c}$$

Since all constraints and the objective function are convex with respect to the variables, problem (34) constitutes

a standard convex program and can be efficiently solved using off-the-shelf solvers. The iterative procedure for solving problem (34) is shown in Algorithm 1.

### Algorithm 1 Iterative Optimization for Solving Problem (34)

- 1: Set the iteration number  $e = 1$ , and randomly initialize  $\mathbf{W}_{n_c, n_s}^{(0)}$  and  $\mathbf{Q}_{n_c, n_s}^{(0)}$ .
- 2: **repeat**
- 3:   Solve (34) to obtain  $\mathbf{W}_{n_c, n_s, k}$  and  $\mathbf{Q}_{n_c, n_s}$ .
- 4:   Update  $\mathbf{W}_{n_c, n_s, k}^{(e)} = \mathbf{W}_{n_c, n_s, k}$  and  $\mathbf{Q}_{n_c, n_s}^{(e)} = \mathbf{Q}_{n_c, n_s}$ .
- 5:   Calculate  $\bar{\mathbf{W}}_{n_c, n_s}^{(e)}$ ,  $\bar{\mathbf{W}}^{(e)}$ , and  $\bar{\mathbf{Q}}^{(e)}$  using  $\mathbf{W}_{n_c, n_s, k}^{(e)}$  and  $\mathbf{Q}_{n_c, n_s}^{(e)}$ .
- 6:    $e = e + 1$ .
- 7: **until**  $\left\| \bar{\mathbf{W}}_{n_c, n_s}^{(e)} - \bar{\mathbf{W}}_{n_c, n_s}^{(e-1)} \right\| \leq \epsilon$  and  $\left\| \mathbf{Q}_{n_c, n_s}^{(e)} - \mathbf{Q}_{n_c, n_s}^{(e-1)} \right\| \leq \epsilon$ .
- 8: Apply Gaussian randomization to find rank-one solutions  $\mathbf{w}_{n_c, n_s, k}$  based on  $\mathbf{W}_{n_c, n_s, k}$ , and  $\mathbf{q}_{n_c, n_s}$  based on  $\mathbf{Q}_{n_c, n_s}$ .

## V. SIMULATION RESULTS

This section presents numerical results that evaluate the performance of the proposed dual-secure ISAC framework. Unless otherwise specified, all simulation parameters follow the default values listed in Table II. A uniform linear array (ULA) with half-wavelength antenna spacing is employed at the BS, and quadrature phase-shift keying (QPSK) modulation is adopted, i.e., the constellation set  $\mathcal{S}$  corresponds to QPSK. The AG profiles in (22) and (23) are configured at  $(0, 5, 62^\circ)$ ,  $(0, 2, 35^\circ)$ , and  $(3, 4, 40^\circ)$ . The BS is located at  $(0, 0)$ , the sensing Eve at  $(3, 1)$ , and the sensing target at  $(12, 11)$  with a velocity of 46 m/s. Two CUs are located at  $(15, -1)$

$$\begin{aligned}
 & \frac{1}{N_c N_s} \sum_{n_c \in \mathcal{N}_c, n_s \in \mathcal{N}_s} \log \det \left( \mathbf{H}_{n_c, n_s, k} \left( \sum_{k' \in \mathcal{K}} \mathbf{W}_{n_c, n_s, k'} + \mathbf{Q}_{n_c, n_s} \right) \mathbf{H}_{n_c, n_s, k}^H + \sigma_c^2 \mathbf{I} \right) \\
 & + \log \det \left( \mathbf{H}_{n_c, n_s, m_c} \left( \sum_{\substack{k' \in \mathcal{K}, \\ k' \neq k}} \mathbf{W}_{n_c, n_s, k'} + \mathbf{Q}_{n_c, n_s} \right) \mathbf{H}_{n_c, n_s, m_c}^H + \sigma_c^2 \mathbf{I} \right) \\
 & - \log \det (\Xi_{n_c, n_s, k}) - \text{Tr} \left( \Xi_{n_c, n_s, k}^{-1} \left( \Xi_{n_c, n_s, k} - \mathbf{H}_{n_c, n_s, k} \left( \sum_{\substack{k' \in \mathcal{K}, \\ k' \neq k}} \mathbf{W}_{n_c, n_s, k'} + \mathbf{Q}_{n_c, n_s} \right) \mathbf{H}_{n_c, n_s, k}^H - \sigma_c^2 \mathbf{I} \right) \right) \\
 & - \log \det (\Xi_{n_c, n_s, m_c}) - \text{Tr} \left( \Xi_{n_c, n_s, m_c}^{-1} \left( \Xi_{n_c, n_s, m_c} - \mathbf{H}_{n_c, n_s, m_c} \left( \sum_{k' \in \mathcal{K}} \mathbf{W}_{n_c, n_s, k'} + \mathbf{Q}_{n_c, n_s} \right) \mathbf{H}_{n_c, n_s, m_c}^H - \sigma_c^2 \mathbf{I} \right) \right) \geq \eta_s, \tag{33}
 \end{aligned}$$

where  $\Xi_{n_c, n_s, k} = \mathbf{H}_{n_c, n_s, k} \left( \sum_{\substack{k' \in \mathcal{K}, \\ k' \neq k}} \mathbf{W}_{n_c, n_s, k'}^{(e)} + \mathbf{Q}_{n_c, n_s}^{(e)} \right) \mathbf{H}_{n_c, n_s, k}^H + \sigma_c^2 \mathbf{I}$ ,  $\Xi_{n_c, n_s, m_c} = \mathbf{H}_{n_c, n_s, m_c} \left( \sum_{k' \in \mathcal{K}} \mathbf{W}_{n_c, n_s, k'}^{(e)} + \mathbf{Q}_{n_c, n_s}^{(e)} \right) \mathbf{H}_{n_c, n_s, m_c}^H + \sigma_c^2 \mathbf{I}$ .

 TABLE II  
 SIMULATION SETTINGS

Parameter	Symbol	Value
Carrier frequency	$f_c$	24 GHz
OFDM symbol duration	$T$	$8.33 \times 10^{-6}$
Cyclic prefix duration	$T_{\text{CP}}$	$0.59 \times 10^{-6}$
Number of subcarriers	$N_c$	12
Number of symbols	$N_s$	8
Number of transmit/receive antennas	$N_t, N_r$	16
Sensing Eve's receive antennas	$N_{m_r}$	24
Communication noise power	$\sigma_c^2$	-70 dBm
Sensing noise power	$\sigma_r^2$	-70 dBm
Power budget	$P_t$	50 dBm

and  $(9, -4)$ , respectively, while the communication Eve is located at  $(2, -8)$ . Unless otherwise stated, the sensing Eve is assumed to have perfectly recovered the reference signal, i.e.,  $\hat{\mathbf{x}}_{n_c, n_s} = \mathbf{x}_{n_c, n_s}$ . Each communication Eve and each CU is equipped with two antenna elements. All channels are modeled using geometry-based channel models with free-space path loss.

#### A. Four-Way Trade-Offs Enabled by Artificial Ghosts

In this subsection, we investigate how the design of AGs affects the sensing performance, sensing security, communication performance, and communication security. We first examine the impact of the ISL. As shown in Fig. 3, for a fixed value of  $\eta_{\text{PSL}}$  and  $\eta_{\text{ISL}}$ , increasing the secrecy rate requirement

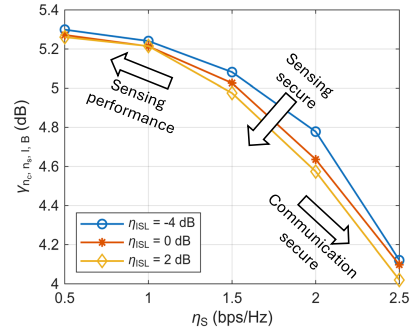


Fig. 3. The sensing SNR for BS ( $\gamma_{n_c, n_s, l, B}$ ) versus the secrecy rate for users ( $\eta_S$ ). The values of  $\eta_{\text{PSL}}$  is set to -25 dB and  $\eta_E = 3$  bps/Hz.

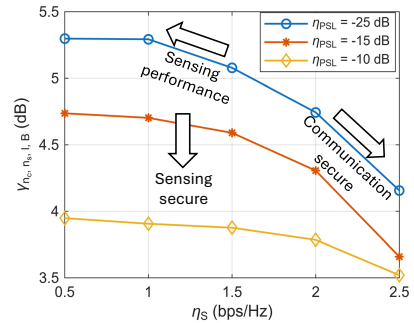


Fig. 4. The sensing SNR for BS ( $\gamma_{n_c, n_s, l, B}$ ) versus the secrecy rate for users ( $\eta_S$ ). The values of  $\eta_{\text{ISL}}$  is set to -4 dB and  $\eta_E = 5$  bps/Hz.

$\eta_S$  leads to a reduction in the sensing SNR at the BS. This indicates that achieving higher communication security comes at the cost of degraded sensing performance. The underlying reason is that stricter communication security requirements demand more transmit power to be allocated toward the CUs, thereby reducing the resources available for coherent sensing. From the communication perspective, communication performance improves with increasing communication security, since both metrics benefit from higher signal power directed toward the legitimate users. This reveals an inherent trade-off among sensing performance, communication performance, and

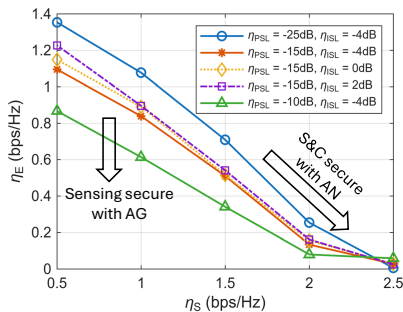


Fig. 5. The sensing Eve reference signal transmission rate ( $\eta_E$ ) versus user secrecy rate ( $\eta_S$ ).

communication security, where enhanced communication performance and security inevitably degrade sensing performance. Notably, increasing the ISL, e.g., from  $-4$  dB to  $2$  dB, further reduces the sensing SNR when the communication security level is fixed. A larger ISL allows more energy to be distributed over sidelobes, which enhances sensing security. However, this sidelobe energy leakage reduces the power available for both coherent sensing at the BS and transmission toward the CUs, thereby degrading communication performance and communication security. Consequently, increasing the ISL simultaneously deteriorates sensing performance, communication performance, and communication security, while improving sensing security.

In Fig. 4, we investigate the impact of the PSL. Similar to the observations in Fig. 3, for fixed values of  $\eta_{PSL}$  and  $\eta_{ISL}$ , increasing the secrecy rate requirement  $\eta_S$  leads to a reduction in the sensing SNR at the BS, indicating that enhanced communication performance and security is achieved at the expense of sensing performance. Moreover, increasing the PSL threshold, e.g., from  $-25$  dB to  $-10$  dB, improves sensing security by strengthening the sidelobes that represent the AGs. However, when the communication secrecy rate is fixed, a larger PSL results in a noticeable degradation of the sensing SNR. This is because a higher PSL permits stronger sidelobe levels to realize more prominent AGs, which consumes additional transmit power and reduces the energy that can be coherently focused on sensing. As a result, less power is available to ensure high sensing performance at the BS.

#### B. Four-Way Trade-Offs Enabled by Artificial Noise

In this subsection, we focus on the impact of AN. As shown in Fig. 5, for fixed values of  $\eta_{PSL}$  and  $\eta_{ISL}$ , increasing the secrecy rate requirement  $\eta_S$  leads to a reduction in the sensing Eve's reference signal transmission rate  $\eta_E$ . This indicates that enhancing communication security simultaneously improves sensing security under the AN-assisted design. The reason is that stricter secrecy requirements necessitate injecting more AN to suppress potential communication eavesdroppers, which also degrades the reference signal quality received at the sensing Eve. For fixed values of  $\eta_{ISL}$  and  $\eta_S$ , increasing the PSL threshold results in a further reduction of  $\eta_E$ . This is because allocating more transmit power to sidelobe shaping

for AGs generation reduces the effective beamforming gain toward the sensing Eve, thereby lowering the achievable reference signal rate. By contrast, when  $\eta_{PSL}$  and  $\eta_S$  are fixed, increasing  $\eta_{ISL}$  leads to a slight increase in  $\eta_E$ . This occurs since higher ISL permits additional sidelobe energy that is not exclusively associated with the AGs, allowing the sensing Eve to opportunistically collect part of this leaked energy. Overall, the AN design effectively enhances communication performance and security, as well as sensing security by degrading the sensing Eve's reference signal. However, this comes at the cost of reduced sensing performance at the BS due to the additional power allocated to AN. When combined with AG-based sidelobe shaping, sensing security can be further strengthened, while incurring an additional trade-off against sensing performance if the same communication performance and secrecy requirements are to be maintained.

#### C. Detection Performance at the BS and Sensing Eve

In this subsection, we investigate the correct detection probability, which is defined as the ratio between the number of detected true targets and the total number of detected targets, including both true and ghost targets. This metric enables a direct evaluation of the impact of AGs on sensing security.

Target detection is performed using a constant false alarm rate (CFAR) detector with a false alarm probability of  $10^{-5}$ . Two types of reference signals available at the sensing Eve are considered. The first corresponds to an ideal scenario in which the transmitted waveform is perfectly recovered, i.e.,  $\mathbf{H}_{r,m_r}^H \mathbf{H}_{r,m_r} = \mathbf{I}$ , leading to  $\hat{\mathbf{x}}_{n_c, n_s} = \mathbf{x}_{n_c, n_s}$ . The second represents a more practical case where the reference signal is recovered using an MVU estimator shown in (11), in which path loss and channel effects cannot be completely eliminated. As shown in Fig. 6(a), increasing the PSL threshold  $\eta_{PSL}$  results in a monotonic reduction in detection probability for all receivers. This behavior arises because a larger PSL permits stronger sidelobes representing the AGs. These AGs are more likely to trigger the CFAR detector, thereby increasing false detection and reducing the probability of correctly identifying true targets. This observation is consistent with the previous results and confirms that enhancing sensing security via AGs inevitably degrades sensing performance.

For a fixed PSL value, e.g.,  $\eta_{PSL} = -15$  dB, the sensing Eve with a perfectly recovered reference signal achieves a higher detection probability than that using the MVU recovered reference. This is because perfect recovery effectively removes the impact of path loss and channel distortion, rendering the sensing Eve less sensitive to AN. Nevertheless, its detection probability remains noticeably lower than that of the BS, indicating that sensing security is still ensured. In contrast, under the MVU-based recovery, residual channel distortion and AN jointly impair the sensing Eve, leading to a further reduction in detection probability and highlighting the effectiveness of AN in practical sensing security enhancement. Similar trends can be observed in Figs. 6(b) and (c).

By comparing Figs. 6(a) and (b), where the sensing Eve's reference signal rate constraint  $\eta_E$  is reduced to impose stricter sensing security, a slight degradation in the detection probability of the sensing Eve is observed for both reference recovery

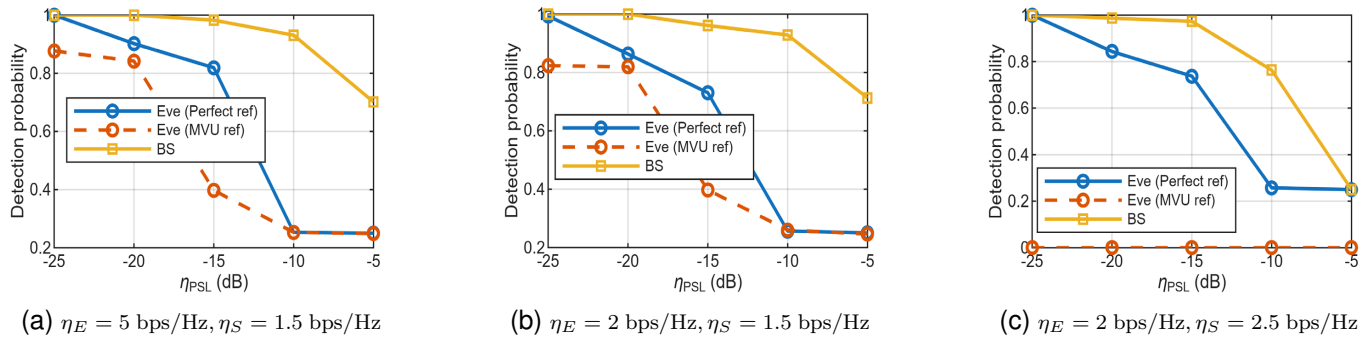


Fig. 6. Detection probability versus  $\eta_{\text{PSL}}$  under different design parameters. Two types of sensing Eve reference signals are considered: an MVU-based reference signal and an idealized reference signal assuming perfect cancellation of the channel matrix.

methods. Meanwhile, a marginal reduction in the BS detection probability is also observed, indicating that improving sensing security via AN incurs a trade-off with sensing performance, in agreement with the four-way trade-off analysis presented earlier. Furthermore, by comparing Figs. 6(b) and (c), where the communication secrecy requirement  $\eta_S$  is increased, the BS experiences a slight degradation in detection probability. This result further corroborates that enhanced communication performance and security are achieved at the expense of sensing performance. For the sensing Eve, increasing  $\eta_S$  also reduces the detection probability under perfect reference recovery, since more transmit power is allocated to secure communication, leaving less signal energy observable by the sensing Eve. Under the MVU-based reference recovery, the detection probability drops to nearly zero, as the combined effects of AN, path loss, and residual channel distortion severely limit the sensing Eve's coherent processing capability.

In summary, the results demonstrate that AGs and AN jointly enable effective sensing security by significantly degrading the detection capability of sensing Eves under both ideal and practical reference recovery scenarios. However, these security gains are accompanied by unavoidable trade-offs with sensing performance at the BS, particularly when stricter sensing or communication secrecy requirements are imposed.

#### D. Visual Comparison of Secure and Non-Secure Sensing

In this subsection, we present the delay-Doppler (DD) maps observed at the BS and the sensing Eve to visually illustrate the effects of the proposed dual-secure ISAC design. By setting  $\bar{\mathbf{A}}^{\text{H}}(\hat{\theta}_{l,t}) = \bar{\mathbf{A}}^{\text{H}}(\theta_{l,t})$  in (22), the resulting function exhibits a periodic structure in the DD domain. The AG profile is set to  $(\Delta\ell, \Delta\nu) = (3, 4)$ . A baseline design without sensing security is also included for comparison.

By comparing Figs. 7(a) and (d), it can be observed that the BS DD map under the proposed secure design exhibits a higher noise floor than that of the non-secure baseline. This behavior is mainly attributed to the trade-off between sensing performance and sensing security, where part of the transmit power is intentionally allocated to AN injection and sidelobe shaping for AGs, resulting in a reduced sensing SNR at the BS. Nevertheless, the true target remains clearly identifiable,

indicating that reliable sensing performance can still be maintained under the proposed design. Further background noise suppression may be achieved by applying more advanced signal processing or filtering techniques at the BS. By comparing Figs. 7(b) and (e), it is evident that under the proposed secure design, periodic AGs emerge in the sensing Eve's DD map, whereas the non-secure baseline primarily highlights the true target. This contrast demonstrates that the baseline design is vulnerable to sensing eavesdropping, while the proposed design effectively enhances sensing security by misleading the sensing Eve with AGs. A comparison between Figs. 7(a) and (b) further reveal that the AGs are only observable in the sensing Eve's DD map and are absent from the BS DD map. This confirms that the proposed design degrades the sensing capability of the Eve without introducing AGs at the BS.

Further, by comparing Figs. 7(c) and (f), it can be seen that AN severely impairs the sensing Eve's detection capability under MVU-based reference recovery. The impact of AN is further amplified by the residual channel matrix, resulting in a significantly elevated noise floor and obscured target signatures. In contrast, although the non-secure design exhibits some background noise due to residual channel effects, the true target remains distinguishable, which poses potential sensing security risks. Finally, as shown in Fig. 8, in the presence of multiple targets, the AGs remain preserved and observable by the sensing Eve, demonstrating the robustness of the proposed design in multi-target scenarios.

Fig. 9 illustrates the AGs generated in the delay-angle (DA) domain, where the AG locations are set to  $(5^\circ, 2)$  and  $(5^\circ, 5)$ . As shown in Fig. 9(b), these AGs are clearly observable in the sensing Eve's DA map, thereby degrading its target detection capability and reducing the probability of correct detection. In contrast, although the AGs are also present in the BS's DA profile in Fig. 9(a), their impact on legitimate sensing is negligible. This is because, under **Assumption 3**, the BS has prior knowledge of the true target angles, enabling it to identify and suppress the AGs in the angle domain, thus preserving the sensing performance. Overall, the results demonstrate the effectiveness of the proposed dual-secure design and indicate that the joint use of AN and AG is essential to simultaneously guarantee sensing security and communication security in ISAC systems.

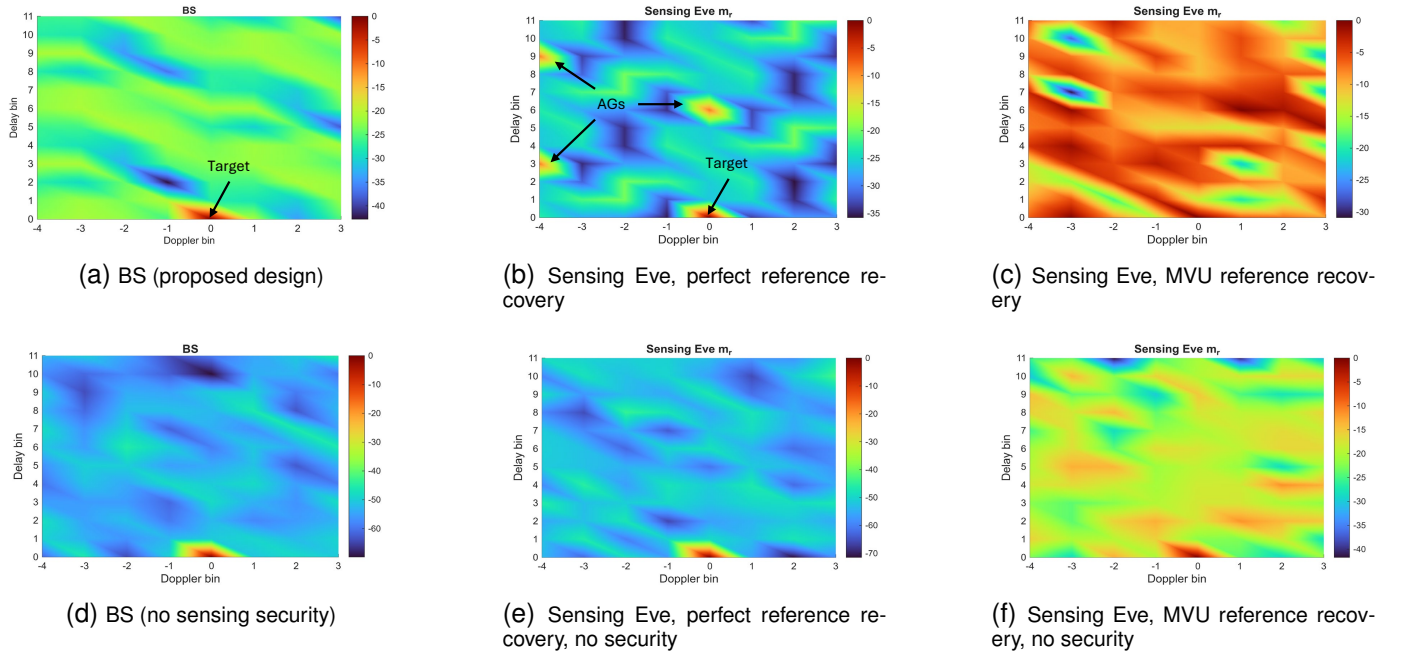


Fig. 7. Delay-Doppler maps observed at the BS and sensing Eve  $m_r$  under the proposed dual-secure ISAC design and a baseline without security. Two reference signal recovery cases are considered for the sensing Eve. In (b) and (e), the sensing Eve is located at (3, 1), whereas in (c) and (f), it is located at (30, 10). Other parameters are set as  $\eta_{PSL} = -10$  dB,  $\eta_{ISL} = -4$  dB,  $\eta_E = 2$  bps/Hz,  $\eta_S = 1.5$  bps/Hz.

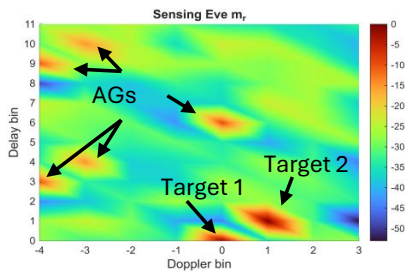


Fig. 8. Delay-Doppler map of target 1 observed by sensing Eve  $m_r$  in the presence of two targets. Target 2 has a coordinate of (85, 42) with a velocity of 120 m/s.

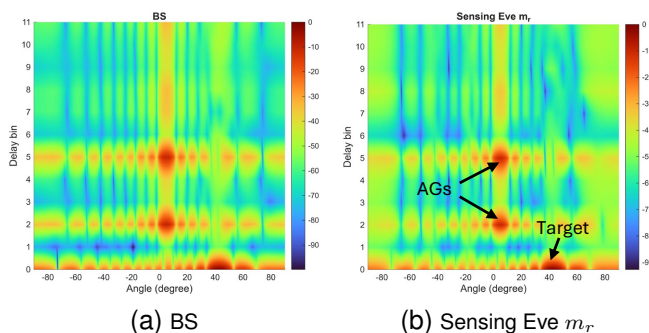


Fig. 9. Delay-angle maps observed at the BS and sensing Eve  $m_r$  under the proposed dual-secure ISAC design. Other parameters are set as  $\eta_{PSL} = -10$  dB,  $\eta_{ISL} = -4$  dB,  $\eta_E = 2$  bps/Hz,  $\eta_S = 1.5$  bps/Hz.

## VI. CONCLUSION

In this paper, we proposed a dual-secure design to mitigate both sensing and communication eavesdropping in MIMO-OFDM ISAC systems without requiring the CSI of the

Eves. Signal models were established for the BS, legitimate communication users, sensing Eves, and communication Eves. To ensure communication security and sensing security, AN was first introduced through transmit beamforming to generate interference at communication Eves and to limit the estimation capability of sensing Eves. This mechanism constitutes the first layer of defense. When sensing Eves are located close to the BS or the targets, their sensing capability may remain strong despite AN injection. To address this scenario, a second layer of protection was developed by intentionally generating AGs with fake angle-range-velocity profiles that are observable only by sensing Eves. As a result, the probability of correctly detecting the true targets is significantly reduced. To realize the proposed two-layer protection, the transmit beamformers were optimized to maximize the sensing SNR at the BS while satisfying multiple security and performance constraints, including a minimum secrecy rate for legitimate users, a maximum allowable data rate at the sensing Eves to degrade the quality of its reference signal, and PSL and ISL constraints for AG generation. Numerical results demonstrated the effectiveness of the proposed framework and revealed the inherent trade-offs among communication performance, communication security, sensing performance, and sensing security.

## REFERENCES

- [1] F. Liu, Y. Cui, C. Masouros, J. Xu, T. X. Han, Y. C. Eldar, and S. Buzzi, "Integrated sensing and communications: Toward dual-functional wireless networks for 6g and beyond," *IEEE journal on selected areas in communications*, vol. 40, no. 6, pp. 1728–1767, 2022.
- [2] K. Meng, C. Masouros, A. P. Petropulu, and L. Hanzo, "Cooperative isac networks: Opportunities and challenges," *IEEE Wireless Communications*, vol. 32, no. 3, pp. 212–219, 2025.

- [3] Z. Du, F. Liu, Y. Li, W. Yuan, Y. Cui, Z. Zhang, C. Masouros, and B. Ai, "Toward isac-empowered vehicular networks: Framework, advances, and opportunities," *IEEE Wireless Communications*, vol. 32, no. 2, pp. 222–229, 2025.
- [4] Y. Yang, Y. Ding, Z. Yang, C. Huang, Z. Zhang, D. Niyato, and M. Shikh-Bahaei, "Toward efficient and privacy-aware ehealth systems: An integrated sensing, computing, and semantic communication approach," *IEEE Internet of Things Journal*, 2025.
- [5] X. Zhu, J. Liu, L. Lu, T. Zhang, T. Qiu, C. Wang, and Y. Liu, "Enabling intelligent connectivity: A survey of secure isac in 6g networks," *IEEE Communications Surveys & Tutorials*, 2024.
- [6] X. Luo, Q. Lin, R. Zhang, H.-H. Chen, X. Wang, and M. Huang, "Isac—a survey on its layered architecture, technologies, standardizations, prototypes and testbeds," *IEEE Communications Surveys & Tutorials*, 2025.
- [7] N. Su, F. Liu, and C. Masouros, "Sensing-assisted eavesdropper estimation: An isac breakthrough in physical layer security," *IEEE Transactions on Wireless Communications*, vol. 23, no. 4, pp. 3162–3174, 2023.
- [8] F. Liu, Y.-F. Liu, Y. Cui, C. Masouros, J. Xu, T. X. Han, S. Buzzi, Y. C. Eldar, and S. Jin, "Sensing with communication signals: From information theory to signal processing," *arXiv preprint arXiv:2502.10819*, 2025.
- [9] N. Su, F. Liu, and C. Masouros, "Secure radar-communication systems with malicious targets: Integrating radar, communications and jamming functionalities," *IEEE Transactions on Wireless Communications*, vol. 20, no. 1, pp. 83–95, 2020.
- [10] F. Jia, A. Li, X. Liao, Y. Li, and C. Masouros, "Secure precoding via interference exploitation in integrated sensing and communication system," *IEEE Wireless Communications Letters*, 2025.
- [11] J. Chu, R. Liu, M. Li, Y. Liu, and Q. Liu, "Joint secure transmit beamforming designs for integrated sensing and communication systems," *IEEE Transactions on Vehicular Technology*, vol. 72, no. 4, pp. 4778–4791, 2022.
- [12] F. Xia, Z. Fei, X. Wang, N. Su, Z. Wang, Y. Liu, and J. Xu, "Towards secure isac beamforming: How many dedicated sensing beams are required?" *arXiv preprint arXiv:2510.03749*, 2025.
- [13] W. Zhou, R. Zhang, G. Chen, and W. Wu, "Integrated sensing and communication waveform design: A survey," *IEEE Open Journal of the Communications Society*, vol. 3, pp. 1930–1949, 2022.
- [14] J. Zhang, S. Guo, S. Gong, C. Xing, N. Zhao, D. W. K. Ng, and D. Niyato, "Intelligent waveform design for integrated sensing and communication," *IEEE Wireless Communications*, 2024.
- [15] H. Pirayesh and H. Zeng, "Jamming attacks and anti-jamming strategies in wireless networks: A comprehensive survey," *IEEE Communications Surveys & Tutorials*, vol. 24, no. 2, pp. 767–809, 2022.
- [16] Y. Liu, B. Zhang, D. Guo, H. Zhang, G. Ding, N. Yang, and J. Gu, "A game theoretical anti-jamming beamforming approach for integrated sensing and communications systems," *IEEE Transactions on Vehicular Technology*, vol. 73, no. 10, pp. 15 780–15 785, 2024.
- [17] R. Geng, J. Wang, Y. Yuan, F. Zhan, T. Zhang, R. Zhang, P. Huang, D. Zhang, J. Chen, Y. Hu *et al.*, "A survey of wireless sensing security from a role-based view," *IEEE Communications Surveys & Tutorials*, 2025.
- [18] K. Han, C. Masouros, T. Riihonen, and M. G. Amin, "Next-generation mimo transceivers for integrated sensing and communications: Unique security vulnerabilities and solutions," *arXiv preprint arXiv:2511.20309*, 2025.
- [19] Y. Cao and L. Duan, "Sensing for jamming in isac: Beam scanning and beamforming optimization," *IEEE Transactions on Information Forensics and Security*, vol. 20, pp. 6502–6514, 2025.
- [20] X. Li, Z. Wu, Y. Cai, S. Hu, Y. Liao, and W. Yuan, "Win-win of communication & sensing security for mc-noma isac systems," *IEEE Journal on Selected Areas in Communications*, 2025.
- [21] S. M. Hernandez and E. Bulut, "Scheduled spatial sensing against adversarial wifi sensing," in *2023 IEEE International Conference on Pervasive Computing and Communications (PerCom)*. IEEE, 2023, pp. 91–100.
- [22] X. Meng, J. Zhou, X. Liu, X. Tong, W. Qu, and J. Wang, "Secur-fi: A secure wireless sensing system based on commercial wi-fi devices," in *IEEE INFOCOM 2023 - IEEE Conference on Computer Communications*, 2023, pp. 1–10.
- [23] K. Qu, J. Ye, X. Li, and S. Guo, "Privacy and security in ubiquitous integrated sensing and communication: Threats, challenges and future directions," *arXiv preprint arXiv:2308.00253*, 2023.
- [24] W. Aman, E.-M. Illi, M. Qaraq, and S. Al-Kuwari, "Integrating communication, sensing, and security: Progress and prospects of pls in isac systems," *arXiv preprint arXiv:2505.05090*, 2025.
- [25] H. Jia, R. Zhu, A. Sciarone, and L. Ma, "Illegal sensing suppression for integrated sensing and communication system," *IEEE Internet of Things Journal*, 2024.
- [26] J. Zou, C. Masouros, F. Liu, and S. Sun, "Securing the sensing functionality in isac networks: An artificial noise design," *IEEE Transactions on Vehicular Technology*, vol. 73, no. 11, pp. 17 800–17 805, 2024.
- [27] C. Zhou, Z. Zhang, X. Liu, Y. Xiao, N. Li, Z. Ma, and M. Xiao, "Beamforming design for secure wireless sensing in isac systems," in *2025 IEEE International Conference on Communications Workshops (ICC Workshops)*. IEEE, 2025, pp. 1239–1244.
- [28] Z. Ren, J. Xu, L. Qiu, and D. Wing Kwan Ng, "Secure cell-free integrated sensing and communication in the presence of information and sensing eavesdroppers," *IEEE Journal on Selected Areas in Communications*, vol. 42, no. 11, pp. 3217–3231, 2024.
- [29] A. Musallam and H. Li, "Enhancing sensing privacy in isac through joint signal and artificial noise beamforming," in *ICC 2025-IEEE International Conference on Communications*. IEEE, 2025, pp. 6019–6024.
- [30] K. Han, K. Meng, and C. Masouros, "Sensing-secure isac: Ambiguity function engineering for impairing unauthorized sensing," *IEEE Transactions on Wireless Communications*, 2025.
- [31] B. Du, K. Han, and C. Masouros, "Securing the sensing functionality in isac: Kld-based ambiguity function shaping," *arXiv preprint arXiv:2512.19974*, 2025.
- [32] J. Chen, X. Lei, K. Meng, K. Han, Y. Zhang, C. Masouros, and A. P. Petropulu, "Sensing security in near-field isac: Exploiting scatterers for eavesdropper deception," *arXiv preprint arXiv:2510.20140*, 2025.
- [33] J. Li, G. Zhou, T. Gong, and N. Liu, "A framework for mutual information-based mimo integrated sensing and communication beamforming design," *IEEE Transactions on Vehicular Technology*, vol. 73, no. 6, pp. 8352–8366, 2024.
- [34] Z.-T. Liao, S.-F. Wu, M.-C. Lee, T.-C. Chiu, and T.-S. Lee, "Design of joint transmit beamforming for multi-user mimo-ofdm integrated sensing and communication systems," *IEEE Transactions on Wireless Communications*, 2025.
- [35] C. Sturm and W. Wiesbeck, "Waveform design and signal processing aspects for fusion of wireless communications and radar sensing," *Proceedings of the IEEE*, vol. 99, no. 7, pp. 1236–1259, 2011.
- [36] Q. Dai, Y. Zeng, H. Wang, C. You, C. Zhou, H. Cheng, X. Xu, S. Jin, A. L. Swindlehurst, Y. C. Eldar *et al.*, "A tutorial on mimo-ofdm isac: From far-field to near-field," *arXiv preprint arXiv:2504.19091*, 2025.
- [37] P. Li, M. Li, R. Liu, Q. Liu, and A. L. Swindlehurst, "Mimo-ofdm isac waveform design for range-doppler sidelobe suppression," *IEEE Transactions on Wireless Communications*, 2024.
- [38] R. Schmidt, "Multiple emitter location and signal parameter estimation," *IEEE transactions on antennas and propagation*, vol. 34, no. 3, pp. 276–280, 1986.
- [39] S. M. Kay, *Fundamentals of statistical signal processing: estimation theory*. Prentice-Hall, Inc., 1993.
- [40] X. Wei, W. Yuan, K. Zhang, and F. Liu, "Otsf-assisted isac system: Delay doppler channel estimation and sdr-based implementation," *IEEE Transactions on Mobile Computing*, 2025.
- [41] P. Li, M. Li, R. Liu, Q. Liu, and A. L. Swindlehurst, "Sensing-oriented adaptive resource allocation designs for ofdm-isac systems," *arXiv preprint arXiv:2504.06605*, 2025.
- [42] C.-Y. Chen and P. Vaidyanathan, "Properties of the mimo radar ambiguity function," in *2008 IEEE International Conference on Acoustics, Speech and Signal Processing*. IEEE, 2008, pp. 2309–2312.
- [43] Y. Li, Z. Wei, Y. Cui, and Z. Feng, "A dual function compromise for uplink isac: Joint spectrum and power management," in *2024 IEEE Wireless Communications and Networking Conference (WCNC)*. IEEE, 2024, pp. 1–6.
- [44] H. Niu, Y. Xiao, X. Lei, J. Chen, Z. Xiao, M. Li, and C. Yuen, "A survey on artificial noise for physical layer security: Opportunities, technologies, guidelines, advances, and trends," *IEEE Communications Surveys & Tutorials*, 2025.
- [45] Z. Xiao, R. Liu, M. Li, W. Wang, and Q. Liu, "Sparsity exploitation via joint receive processing and transmit beamforming design for mimo-ofdm isac systems," *IEEE Transactions on Communications*, 2024.
- [46] Y. Yang, J. Zhou, Z. Yang, and M. Shikh-Bahaei, "Fluid antenna-enabled near-field integrated sensing, computing and semantic communication for emerging applications," *IEEE Transactions on Cognitive Communications and Networking*, 2025.
- [47] Y. Sun, P. Babu, and D. P. Palomar, "Majorization-minimization algorithms in signal processing, communications, and machine learning," *IEEE Transactions on Signal Processing*, vol. 65, no. 3, pp. 794–816, 2016.